MutBug: A Lightweight and Compact Crawling Robot That Can Run on Both Sides

Tae-Yeon Kim, Chan Kim, Sung-Hyun Kim, and Gwang-Pil Jung

***Abstract*—Double-sided crawling robots have potential to be quite useful for real-world applications. For example, double-sided crawling robots keep crawling even when they are turned over. In this letter, we present a lightweight and compact crawling robot that can run on both sides. To make this possible, two design strategies are proposed: the shared hip joints and the low profile differential drive based on orthogonally oriented four-bars. The shared hip joints allow the robot to have a thin body by reducing redundant structures. The orthogonally oriented four-bars, which can be installed in the limited thin body structure, enable the robot to equally transmit the motor's crank motion to the multiple legs. Thanks to these design strategies, the robot not only has compact size but also successful alternating gait. In result, the MutBug has body thickness of 15 mm and runs at the maximum speed of 0.53 m/s.**

***Index Terms*—Biologically-inspired robots, mechanism design, crawling robot, double-sided crawling.**

I. Introduction

SMALL-SCALE robots have been widely studied due to its ability to maneuver small spaces and narrow gaps where large-scale robots cannot reach. Among small-scale robots, legged types have been preferred due to its obstacle overcoming ability, compared to wheeled robots. RoACH [1], [2], DASH [3], HARM [4], [5], VelociRoACH [6], iSprawl [7], and Mini-Whegs [8] are the representatives of small-scale crawling robots. These robots have shown successful maneuvering performance on various terrains easily seen in daily life.

To utilize small-scale legged robots for real-world applications, however, the robots need to be able to recover posture even when they are turned over. In reality, the robots often roll over while they are overcoming obstacles or falling down. Most of the current small-scale crawling robots have trouble recovering their posture to keep crawling. To solve this issue, some researchers have proposed robots with recovering ability. Li *et al.* [9] invented a wing opening linkages for dynamic terrestrial self-righting inspired by the winged discoid cockroach. Jung *et al.* [10] proposed a jumping-crawling robot that can achieve self-righting from upside-down orientation. Casarez *et al.* [11] installed a single degree of freedom low-mass tail, which gives the robot the capability to dynamically self-right.

The other approach is to make the robot crawl on both sides, like Table I Thanks to the ability of double-sided crawling, these robots can keep moving even when they are turned over. To make this possible, researchers have proposed various designs that focus on two issues. The first is how to create a compact body structure. For example, a thick and bulky body requires large size wheels or wheels at each side. The second is how to transmit the actuator's motion to the multiple legs well while minimizing number of actuators. Minimizing the number of actuators is directly related to compactness of the body structure. If the number of actuators is reduced, then there should be a component that equally transmits the actuator's motion to the multiple legs. Otherwise, the alternating gait is not successfully made and accordingly fails.

Morrey *et al.* [8] proposed the Mini-Whegs that can run on both sides. The robot has a single driving motor to operate two axles and four wheels. Two axles are connected via non-slipping steel drive chains to transmit the motor's motion. Zarrouk *et al.* [12], [13] presented RSTAR that can run in a planar configuration such as upright, or inverted. The robot has thin body and changes the sprawl angle from positive 60 degrees to negative 90 degrees. The RSTAR has three geared spoke wheels at each side and a single motor operates the wheels at each side. These robots have shown great performance of double-sided crawling but, they tend to be a bit weighty since all components are based on conventional mechanical parts.

To make a lightweight robot, Lee *et al.* [14] employed the smart composite microstructures (SCM) process [15] that replaces rigid links and pin joints with composite links and flexure joints. Thanks to the process, the robot weighs only 26.4g. Regarding crawling speed, however, the robot is not very excellent since the leg mechanism is based on a crank-slider and this results in high vertical reaction force. Therefore, the robot tends to have high payload capacity rather than fast crawling speed.

In this letter, we propose a compact and lightweight double-sided crawling robot with improved running speed, as shown in Fig. 1. The MutBug weighs 26.5g and has thin structure as 15mm, achieving double-sided crawling with the maximum speed of 0.53 m/s. Key working principles are the shared hip joints and the low profile differential drive. The shared hip joints

Manuscript received September 3, 2018; accepted December 28, 2018. Date of publication January 29, 2019; date of current version February 15, 2019. This letter was recommended for publication by Associate Editor D. Lau and Editor P. Rocco upon evaluation of the reviewers' comments. This letter was supported in part by the National Research Foundation under Grant NRF-2016R1A5A1938472 and in part by the Defense Acquisition Program Administration under Grant UD130070ID to Bio-Mimetic Robot Research Center. *(Corresponding author: Gwang-Pil Jung.)*

The authors are with the Department of Mechanical and Automotive Engineering, SeoulTech, Seoul 01811, South Korea (e-mail: kimksik2@gmail.com; iopn1213@gmail.com; wkftodrlstjdgusdl@gmail.com; gpjung@seoultech.ac.kr).

This letter has supplementary downloadable material available at http://ieeexplore.ieee.org, provided by the authors.

Digital Object Identifier 10.1109/LRA.2019.2895896

TABLE I
MILLI-SCALE DOUBLE-SIDED CRAWLING ROBOTS

	Size (mm)	Mass (g)	Max. Speed (m/s)	Actuators	Motion Transmission
CardBot	85 x 19	26.4	0.25	2 driving DC motor	Multiple legs connected to a single slider
RSTAR	150	308	1.0	2 driving DC motors, 1 DC motor (sprawl angle adjust), 1 DC motor (slow crawl)	Serially connected geared spokes
Mini-Wheg	90 x 20	146	0.9	1 driving DC motor, 1 steering servo	Non-slipping steel chain
MutBug	100 x 15	26.5	0.53	2 driving DC motor	Orthogonally oriented four-bars

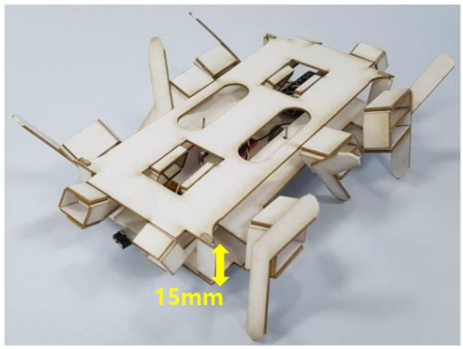

Fig. 1. Double-sided crawling robot. MutBug has 15mm thickness and 26.5g weight.

enable the robot to be thin by reducing the redundant structures. If we simply merge up and down two crawling robots, then the robot tends to be thick and bulky. For the motion transmission in the limited thin body structure, a low profile differential drive is newly developed based on the orthogonally oriented four-bars. This prevents the motion transmitter from deviation induced by external disturbances, which results in transmitting equal motion to the multiple crawling legs and successful alternating gait.

In the following sections, the robot structure and the working principle of MutBug are explained. The modeling section an alyzes the geometric properties to make the robot successfully crawl on both sides. In the experiment section, several crawling tests are done to check the robot's performance for both sides.

II. DESIGN

MutBug has been designed to keep running even when the robot is turned upside down. The simplest solution to do this is to just merge up and down two crawling robots. The whole structure, however, has potential to be bulky and heavy. To avoid such design, the first design goal is how to make the robot's body thin and compact. To achieve the first goal, the hip joints are shared and accordingly, the overlapping structures are removed.

The second design goal is to create a low profile differential drive that can be used in limited space, which is for equally transmitting the actuator motion to the multiple crawling legs. If the differential drive is wrongly designed, then the actuator force is focused on a certain crawling leg and this leads to failure in crawling. To solve this issue, orthogonally oriented four bars have been utilized, which will be explained soon.

A. Hip Design and Motion Transmitter

Fig. 2 shows the schematic of the crawling robot. The robot has two sets of three hip joints. One set is located at the left side and the other is on the right side. Each hip joint has two

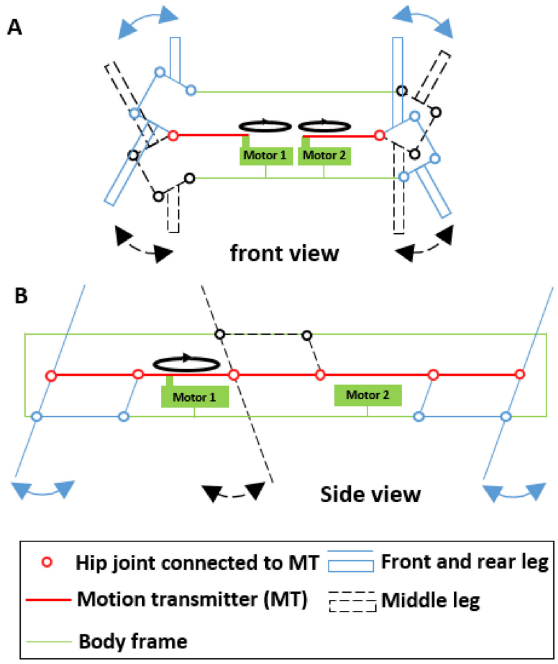

Fig. 2. Schematic of the crawling robot. (a) Front view and (b) side view. Components are explained in the box.

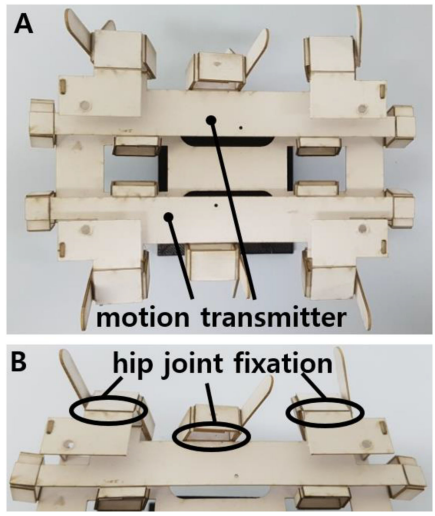

Fig. 3. Design of the MutBug. (a) Motion transmitter and (b) hip joints connected to the motion transmitter.

crawling legs up and down. Therefore, the robot has twelve legs in total.

A hip joint consists of a four-bar linkage to make the crawling motion as shown in Figs. 2 and 3. The four-bar linkages of the hip joints at each side are coupled through a motion transmitter.

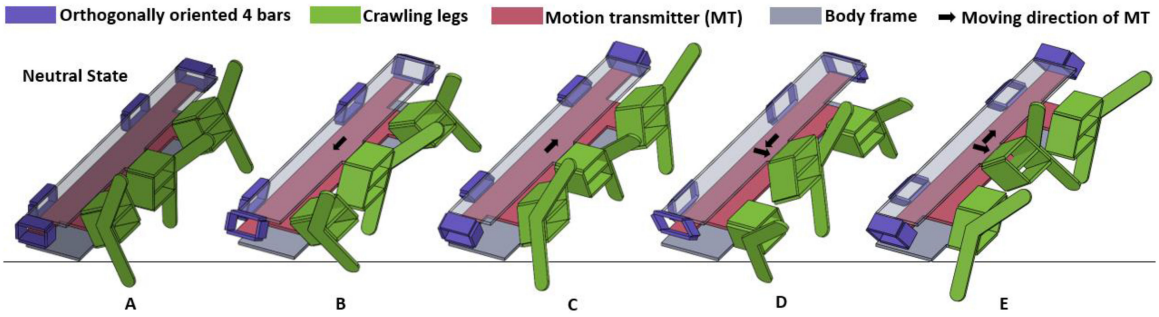

Fig. 4. Orthogonally oriented four-bar prevents the motion transmitter from deviation. (a) The neutral postion of the motion transmitter. The force transmitter moves (b) downward, (c) upward, (d) right and down, and (e) right and up.

The motion transmitter generates the rotating motion originated from the crank connected to the DC motor. That is, a single DC motor operates three hip joints at once.

In Fig. 3, the four-bar linkages of the hip joints are differently attached to the motion transmitter and the body frame. In case of the middle hip joint, the lower part of the four-bar linkage is fixed. On the other hand, the upper part of the four-bar linkage is fixed in case of the hip joints at sides. Due to this design, the hip joints have phase difference of 180 degrees, which enables an alternating gait.

B. Differential Drive Based on Orthogonally Oriented Four-Bars

As previously said, a single DC motor operates three hip joints at once. The problem is how to equally transmit the actuator's rotating motion to the hip joints and the connected crawling legs. If an external force causes a hip joint to be deviated from the actuator's rotating motion, the alternating gait is not successfully generated and accordingly, the crawling gait gets unstable. For this reason, the role of differential drive is substantially important to prevent the motion transmitter from twisting or deviating. That is, the differential drive is required to make the motion transmitter keep rotating while maintaining the correct posture, as shown in Fig. 4.

To solve this issue, DASH [3] and CLASH [16] have used a differential drive composed of two parallel four-bar mechanism. This mechanism allows the robots' hip joints to go through the same angular displacement originated from a single DC motor. Even when an external force is exerted on a leg, all crawling legs maintain the same circular path since the mechanism forces the motion transmitting beams to maintain in parallel. This mechanism has shown great performance to transmit the actuator's motion. In terms of compactness, however, it requires a certain amount of space, which can be problematic in designing this low profile crawling robot.

In order to transmit the actuator motion in limited space, we propose to use orthogonally oriented four-bars shown in Fig. 4. The orthogonally oriented four-bars kinematically couples the crank pin connected to the motor and the motion transmitter. In other words, the orthogonally oriented four-bars allows the crank pin to have a unique corresponding posture of the motion transmitter. Therefore, if a crank pin's position is fixed, then the motion transmitter hardly moves. Thanks to this kinematically coupled relationship, the motion transmitter maintains its posture even when the external disturbances are applied. On the contrary, when the orthogonally oriented four-bars are removed, the crank pin and the motion transmitter become kinematically decoupled. Accordingly, if an external force is exerted on a leg, the motion transmitter is easily distorted as shown in Fig. 5(e) and (f).

To investigate the kinematic relation between the crank pin and the motion transmitter, the position analysis is done as shown in Fig. 5(a)-(d). Based on the parameters of the crawling robot, the position of the crank pin is given as follows:

$$P_c = [-L_9 - L_7(1+\sin\theta_2) + L_c\ L_{hor}/2 - L_7 \sin\theta_1\ L_{ver} - L_7\cos\theta_1], \quad (1)$$

where $L_9 = 1.8$mm, $L_7 = 7$mm, $L_c = 1$mm, $L_{ver} = 13.0$mm, $L_{hor} = 94$mm are the length of body components and θ_1, θ_2 are the tilting angles of the orthogonally oriented four-bars.

Using the Eq. (1), positions of the crank pin are indicated by black-colored circles in Fig. 5(a) and plotted with θ_1 and θ_2 varying from $-30°\sim30°$ and $0°\sim20°$ in 10° increments. As shown in Fig. 5(a), the position of the crank pin varies when the motion transmitter moves. This tells us that the orthogonally oriented four-bars kinematically couples the motion transmitter and the crank pin. In result, the motion originated from the motor can be equally transmitted to multiple crawling legs against external disturbances and finally helps the robot to achieve successful alternating gait.

Moreover, this design allows us to make a thin double-sided crawling robot. The orthogonally oriented four bar has thickness of only 7mm and accordingly, the whole thickness of the robot can be reduced to 15mm.

C. Fabrication

The MutBug consists of 65 links (32 for the orthogonally oriented four-bars, 30 for the legs, 2 for the motion transmitter, 1 for the body) and 96 joints connecting the links. To fabricate and assemble this complex kinematic structure using conventional pin joints and links requires much effort and the structure tends to be heavy because of the increased number of components.

To avoid the issues, the SCM (smart composite microstructures) [15] process is applied. The SCM process replaces the conventional pin joints and links with the flexure joints and

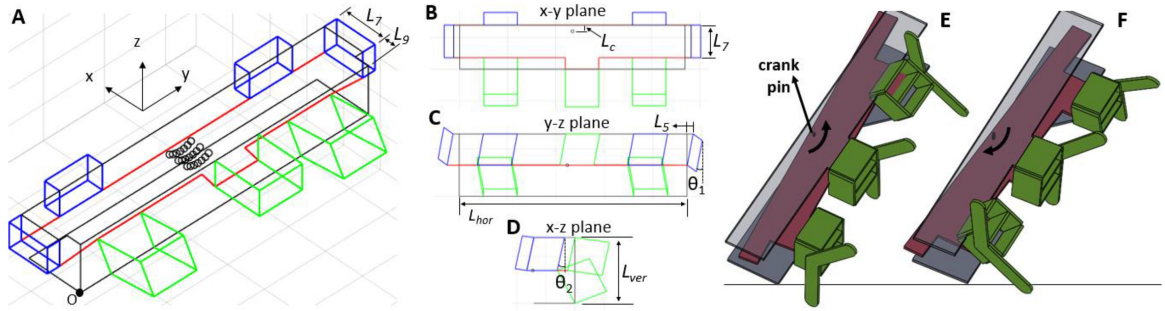

Fig. 5. (a) kinematic model of the crawling robot. The black-colored circles stands for the position of the crank pin. The crank pin's postion is plotted with θ_1 and θ_2 varying from $-30°\sim30°$ and $0°\sim20°$ in $10°$ increments. (b) *x-y* plane view. (c) y-z plane view. (d) x-z plane view. (e), (f) The motion transmitter easily tilts when the orthonogally oriented four-bar is removed.

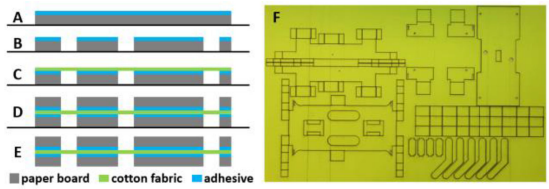

Fig. 6. (a) A paper board with the adhesive on it. (b) The 1st laser cut for flexure joints. (c) Locate the cotton fabric. (d) Locate the equal paper board wih the adhesive (GBC Octive Hot Mount) and align the position of the flexure joints. (e) Lamite the whole layers together (120°C). (f) The laser cut MutBug before folding and assembly.

TABLE II
MASS BUDGET

Components	Quantity (ea.)	Mass (g)	Ratio to overall mass (%)
Body frame	1	11.5	43.8
Transmission	2	8.1	29.8
Control board	1	2.1	7.7
Battery	1	4.5	17.6
Rivet	4	0.3	1.1
Total	-	26.5	100.0

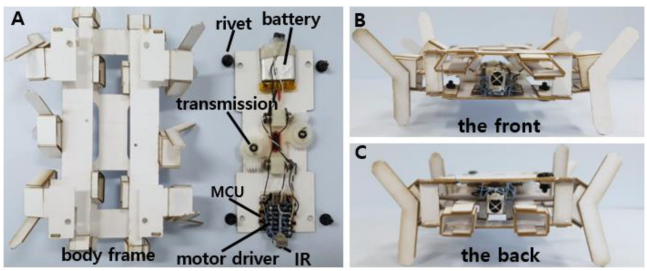

Fig. 7. (a) Componets of the crawling robot. (b) and (c) show the robot's posture in the back and front, respectively.

composite links. In Fig. 6, the whole fabrication process is shown and described. For the MutBug, a paper board ($360\mu m$ thickness) is used as the links and the cotton fabric ($100\mu m$ thickness) is employed as the flexure joints. Thanks to the fabrication process, the frame of the MutBug weighs only 11.5g and the whole robot shows the weight of 26.5g.

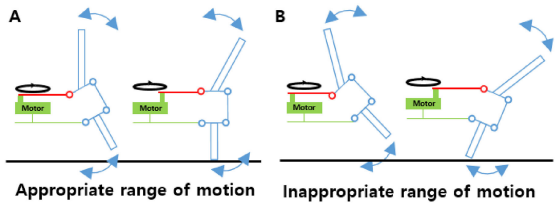

Fig. 8. Range of motion of the hip joints in case of (a) the appropriate and (b) inappropriate settings.

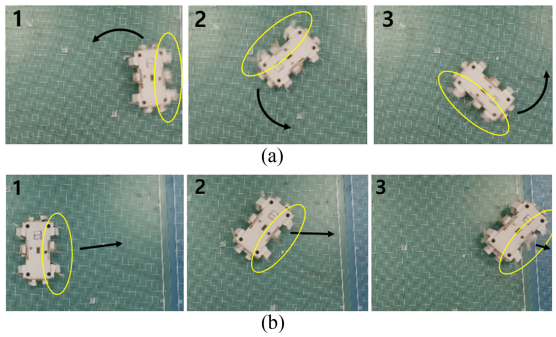

Fig. 9. Moving direction of the crawling robot. When the robot has (a) appropirate range of motion and (b) inapproprate range of motion. The yellow circle and the black-lined arrow indicate the operating legs and the current moving direction.

D. Other Components

The crawler uses two sets of worm gear transmissions operated by brushed DC motors (6 mm diameter, DRC mall). Each transmission is installed at each side and steering can be done by separately controlling the DC motors. The worm gear transmission is thin as 7mm, shown in Fig. 5.

The motors are controlled by changing the PWM ratio and the robot uses the beetle board (DF Robot). The board has an IR communication and a H-bridge motor controller. Whole mass budget of the crawling robot is given in Table I.

III. HIP JOINT AND LEG TRAJECTORY ANALYSIS

A. Hip Joint Range of Motion

MutBug has twelve crawling legs, but uses only six hip joints which are half of the crawling legs. That is, a single hip joint is

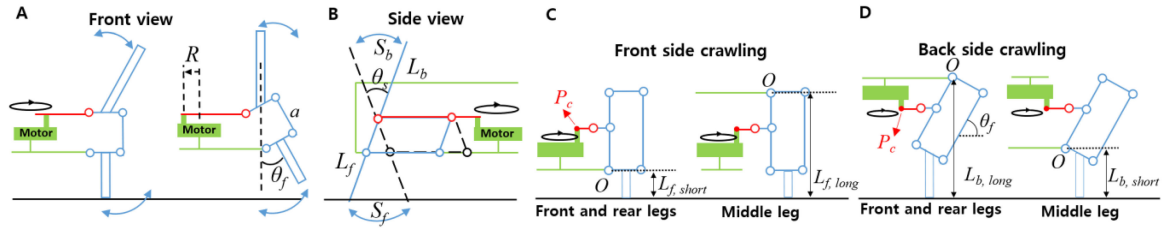

Fig. 10. Parameters for the RoM analysis. (a) front view. (b) side view. (c) front view for the front side crawling and (d) the back side crawling.

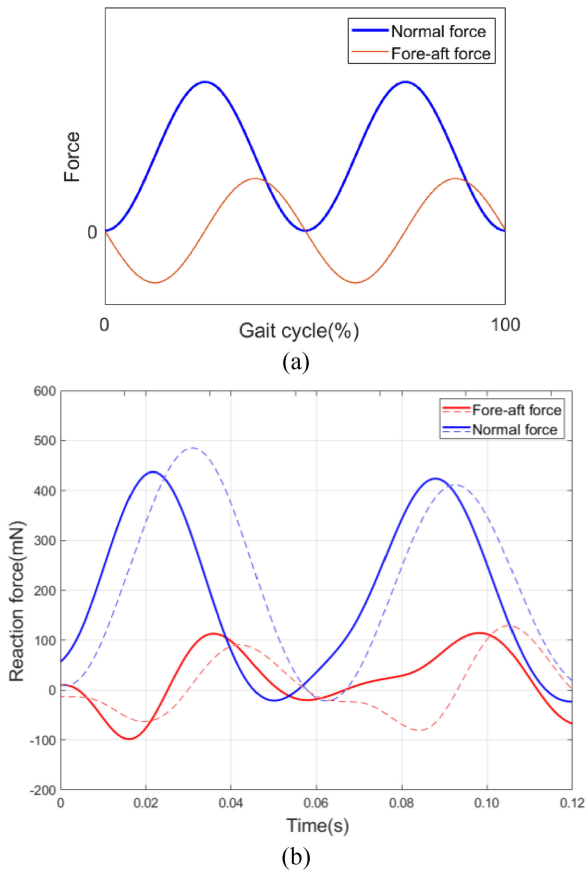

Fig. 11. (a) The SLIP model. (b) Reaction force of the front side crawling (dashed line) and the back side crawling (straight line). The plot indicates one gait cycle.

shared by two crawling legs attached up and down. Since a hip joint is shared by two crawling legs, the movement of a hip joint has influence on the motion of the two crawling legs. Therefore, to analyze and determine the appropriate moving range of the hip joint is important for the robot.

The range of motion (RoM) of a hip joint is basically influenced by the stroke of the crank operated by the motor. For example, incorrect setting of the stroke induces unsuccessful crawling motion as shown in Fig. 8(b). In Fig. 8(b), the crawling leg comes into the robot's body and this causes unnormal gait such as side movement.

Fig. 9(a) and (b) show the crawling of the robot with the proper range of motion and the improper range of motion, respectively. The yellow circles in Fig. 9 indicate the operating legs and the black line stands for the currently moving direction. In Fig. 9(a), the robot operates the legs at right side and has proper range of motion shown in Fig. 8(a). In result, the robot makes a circular path, which is ordinary and predictable moving path. In case of Fig. 9(b), however, the robot moves to the right but hardly shows the rotating motion compared to Fig. 9(a). This is because the legs at right side have the range of motion shown in Fig. 8(b). The legs go to the inside of the robot's body and induces laterally thrusting force. This laterally thrusting force is generated when the legs dig into the body or comes out of the body. As a result, the robot shows unusual movement as shown in Fig. 9(b). Therefore, to select the proper length of the crank and to get the desirable range of motion is important to avoid such phenomenon.

B. Leg Trajectory Analysis

When the motor has the crank arm of the length, *R*, following relations are satisfied as shown in Fig. 10(a) and (b):

$$R \approx a\theta_s \tag{2}$$

$$R \approx a\theta_f, \tag{3}$$

where *R* is the stroke of the crank, *a* is the length of the hip joint, θ_s and θ_f are the angular displacements in the side view and the front view, respectively.

Using, Eq. (2), the length of the foot trajectory for the front side can be estimated as follows:

$$S_f \approx L_f\theta_s = L_f\frac{R}{a}, \tag{4}$$

where S_f is the length of the foot trajectory for the front side, L_f is the length of the leg for the front side.

Unlike the foot trajectory of the front side, the foot trajectory for the back side is given by multiplying the cosine of θ_f as follows:

$$S_b \approx (L_b\theta_s\cos\theta_f)\cos\theta_{\frac{\pi}{2}-f} = \left(L_b\frac{R}{a}\cos\theta_f\right)\cos\theta_{\frac{\pi}{2}-f}, \tag{5}$$

where S_b is the length of the foot trajectory for the back side, L_b is the length of the leg for the back side.

Fig. 10(a) shows the front leg and the back leg that is stuck with a slant. The extent of inclination of the back leg influences the crawling gait. In case of the small θ_f, the foot trajectory of the back side has relatively long stride length, resulting in faster running. However, too small θ_f has potential to induce the failure in alternating gait.

In case of the large θ_f, the foot trajectory for the back side is supposed to have short stride length based on Eq. (5), resulting in slow speed of back side running. If the θ_f gets close to 90 degrees, the foot has zero stride length and the robot cannot

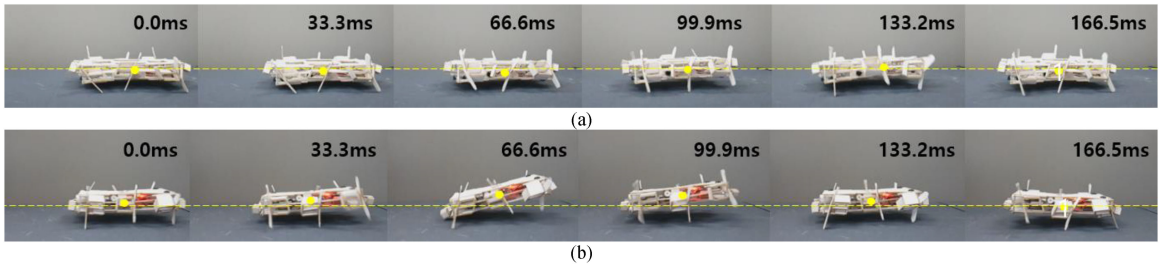

Fig. 12. Running of the crawling robot. (a) The front side crawling and (b) the back side crawling. The yellow dot indicates the mass center of the robot.

even move forward. Based on the analysis, the robot has been designed to have θ_f as 45 degrees. This design enables the robot to have proper stride length to crawl while achieving successful alternating gait on both sides.

The lengths of the legs are determined by estimating and equalizing the total stride length per one gait cycle. To begin with, the length of a leg is defined as the distance from the hip joint to the end of the foot, shown in Fig. 10(c) and (d). The total stride lengths of the front side crawling and the back side crawling are given as Eq. (6) and (7) as follows:

$$S_{f,total} \approx (2L_{f,short} + L_{f,long})\,\theta_s \tag{6}$$

$$S_{b,total} \approx (L_{b,short} + 2L_{b,long})\cos\theta_f \cos\theta_{\pi/2-f}\theta_s, \tag{7}$$

where $\theta_f = 45^\circ$, $L_{f,short} = 8$mm, $L_{f,long} = 24$mm and accordingly, $S_{f,total} = 40\theta_s$.

Since the Eq. (6) and (7) need to be equal, the sum of $L_{b,short}/2$ and $L_{b,long}$ is 40mm. Apart from this condition, the distance from the floor and the robot's underside needs to be maintained while crawling. Based on the conditions, $L_{b,short}$ and $L_{b,long}$ are determined as 16mm and 32mm, respectively $(S_{b,total} = 40\theta_s.)$.

IV. Experimental Results

In this section, the crawling motion and the crawling performance are analyzed by implementing several experiments. The experiments are done by varying the crawling sides to investigate the properties of the double-sided crawling robot.

To analyze the crawling motion, the reaction forces such as the normal force and the fore-aft force are measured for both sides and the results are compared. Also, the crawling images are captured using high speed camera and visually analyzed for both sides. The performance of the crawling robot is shown by testing the robot on messy environments. Through the test, the possibility to use the robot in real-world applications will be shown.

A. Reaction Force Analysis

Crawling motion is analyzed by measuring the reaction forces during one gait cycle. The crawling robot passes over the plate connected to a 3-axis load cell. During running, the normal force and the fore-aft force are measured with the sampling frequency of 2kHz. The experiments are done for both sides of the crawling robot to investigate the differences. Fig. 11(b) shows the measured data after a fifth order of Butterworth filter at a cut off frequency of 160Hz to remove the oscillation of the plate.

To judge whether the MutBug successfully runs, the spring-loaded-inverted pendulum (SLIP) model, which is a classical locomotion template for diverse legged animals [17], has been employed as shown in Fig. 11(a). In the SLIP model, the negative fore-aft force decelerates the robot when the leg initially contacts the ground. As soon as the normal force touches the peak, the fore-aft force starts to accelerate the robot by releasing the stored energy in the spring. In that the MutBug is made of highly compliant materials such as paper boards and flexure joints, the SLIP model can be employed to analyze the crawling motion.

In Fig. 11(b), the normal force and the fore-aft force of the both sides look similar to that of the SLIP model. When the robot initially contacts the ground, the elastic energy is stored in the compliant body structure. At this time, the fore-aft force shows the negative force. The fore-aft force changes to the positive value while the normal force reaches to the peak. The positive fore-aft force, which is the energy releasing phase, thrusts the robot to move forward.

In terms of force magnitude, the force curves of the front side and the back side crawling show similar values. In detail, the back side crawling indicates the peak normal force of 485.1 mN and the peak fore-aft force of 129.2 mN. On the other hand, the front side crawling indicates the peak normal force of 437.4 mN and the peak fore-aft force of 114.8 mN.

From the magnitude and the overall trend of the reaction force curves, we can carefully estimate that the front side crawling and the back side crawling will have a similar speed. In reality, the front side crawling shows a speed of 0.53 m/s and the back side crawls at a speed of 0.51 m/s. This results also corresponds to the leg trajectory analysis in the previous section.

In the previous section, we assume that the running speed of the back side and the front side crawling is dependent on the total stride length, not the total leg length. Following the assumption, the back side legs are designed to be longer compared to the front side legs. Therefore, the both sides have the equal value of the total stride length based on the Eq. (6) and (7). In result, the both sides have an actual stride length of 30mm $(\approx 40\theta_s)$ in total and show similarity in the force curve and the crawling speed.

B. Fluctuation of Mass Center

Fig. 12 shows running of the double-sided crawling robot. Fig. 12(a) and (b) are the front side and the back side crawling, respectively. The yellow dots in Fig. 12 indicate the mass center

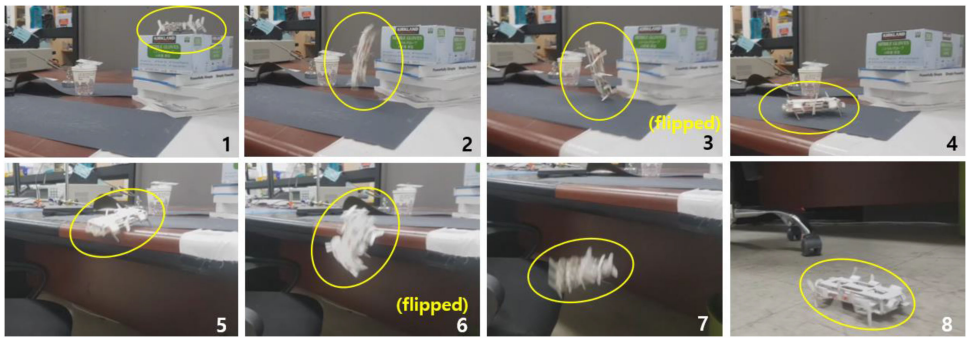

Fig. 13. Possible application of the double-sided crawling robot. The pictures are presented in order as indicated with numbers at bottom right.

of the robot and the yellow line is added to easily understand the fluctuation of the mass center. As shown in Fig. 12, the mass center of the back side crawling fluctuates a bit more, compared to that of the front side crawling. In case of the front side crawling, the mass center fluctuates within about 10 mm in vertical direction. However, the mass center of the back side crawling fluctuates in the range of 20 mm in vertical direction.

Difference in fluctuation of the mass center can be explained based on the reaction force of front side crawling and the back side crawling. In case of the front side crawling, it shows smaller normal force and less fluctuation of the mass center. On the other hand, the back side crawling indicates a bit larger normal force and more fluctuation of the mass center. Due to the difference in the reaction force profile in normal direction, the back side crawling shows slightly unstable crawling compared to the front side crawling.

C. Crawling on Messy Space

The crawling robot is tested on a messy space to show the possibility of use in real world applications. The snapshots of the test are shown in Fig. 13. In the scene no. 1, 2 and 3, the robot crawls forward and flips while the robot falls to the desk 30cm below. After landing, the robot starts to crawl using the back side and approaches to the edge of the desk as shown in the scene no. 4 and 5. In the scene no. 6 and 7, the robot falls to the floor and flips again. As shown in Fig. 13, the MutBug keeps crawling even when it is overturned. In addition, since the robot's body is made of papers and compliant enough, the robot is still operational with no damage after several drops.

V. Conclusion

In this letter, we presented a double-sided crawling robot which is lightweight and compact. To make this possible, two main design strategies are proposed: Shared hip joints and the low profile differential drive based on orthogonally configured four-bars. Sharing the hip joints of the both crawling sides allowed the robot to be thin as 15mm by reducing the overlapping structures. The low profile differential drive for the thin body was possible by orienting the four-bars orthogonally. This enabled the robot to prevent the motion transmitter from deviation induced by external disturbances. Therefore, the motor's crank motion is equally transmitted to the multiple legs and finally the robot successfully achieves alternating gaits. Consequently, the MutBug has thin body as 15mm and crawls with the maximum speed of 0.53m/s on both sides.

References

[1] A. M. Hoover, E. Steltz, and R. S. Fearing, "RoACH: An autonomous 2.4g crawling hexapod robot," in *Proc. IEEE/RSJ Int. Conf. Intell. Robots Syst.*, 2008, pp. 26–33.

[2] A. M. Hoover, S. Burden, X.-Y. Fu, S. S. Sastry, and R. S. Fearing, "Bio-inspired design and dynamic maneuverability of a minimally actuated six-legged robot," in *Proc. IEEE Int. Conf. Biomed. Robot. Biomech.*, 2010, pp. 869–876.

[3] P. Birkmeyer, K. Peterson, and R. S. Fearing, "DASH: A dynamic 16g hexapedal robot," in *Proc. IEEE/RSJ Int. Conf. Intell. Robots Syst.*, 2009, pp. 2683–2689.

[4] A. T. Baisch and R. J. Wood, "Pop-up Assembly of a Quadraupedal Ambulatory MicroRobot," in *Proc. IEEE/RSJ Int. Conf. Intell. Robots Syst.*, 2013, pp. 1518–1524.

[5] A. T. Baisch, O. Ozcan, B. Goldberg, D. Ithier, and R. J. Wood, "High speed locomotion for a quadrupedal microrobot," *Int. J. Robot. Res.*, vol. 33, no. 8, pp. 1063–1082, 2014.

[6] D. W. Haldane and R. S. Fearing, "Running beyond the bio-inspired regime," in *Proc. EEE Int. Conf. Robot. Autom.*, 2015, pp. 4539–4546.

[7] S. Kim, J. E. Clark, and M. R. Cutkosky, "iSprawl: Design and tuning for high-speed autonomous open-loop running," *Int. J. Robot. Res.*, vol. 25, pp. 903–912, 2006.

[8] J. M. Morrey, B. Lambrecht, A. D. Horchler, R. E. Ritzmann, and R. D. Quinn, "Highly mobile and robust small quadruped robots," in *Proc. IEEE/RSJ Int. Conf. Intell. Robots Syst.*, 2003, vol. 1, pp. 82–87.

[9] C. Li, C. C. Kessens, R. S. Fearing, and R. J. Full, "Mechanical principles of dynamic terrestrial self-righting using wings," *Adv. Robot.*, vol. 31, no. 17, pp. 881–900, 2017.

[10] G.-P. Jung, C. S. Casarez, S.-P. Jung, R. S. Fearing, and K.-J. Cho, "An integrated jumping-crawling robot using height-adjustable jumping module," *IEEE Int. Conf. Robot. Autom.*, 2016, pp. 4680–4685.

[11] C. S. Casarez and R. S. Fearing, "Dynamic terrestrial self-righting with a minimal tail," in *Proc. IEEE/RSJ Int. Conf. Intell. Robots Syst.*, 2017, pp. 314–321.

[12] A. P. David Zarrouk, N. Kohut, and R. S. Fearing, "STAR, A sprawl tuned autonomous robot," in *Proc. IEEE Int. Conf. Robot. Autom.*, 2013, pp. 20–25.

[13] D. Zarrouk and L. Yehezkel, "Rising STAR: A highly reconfigurable sprawl tuned robot," *IEEE Robot. Autom. Lett.*, vol. 3, no. 3, pp. 1888–1895, Jul. 2018.

[14] J.-E. Lee, G.-P. Jung, and K.-J. Cho, "Bio-inspired design of a double-sided crawling robot," in *Proc. Conf. Biomimetic Biohybrid Syst.*, 2017, vol. 10384, pp. 562–566.

[15] R. J. Wood, S. Avadhanula, R. Sahai, E. Steltz, and R. S. Fearing, "Microrobot design using fiber reinforced composites," *J. Mech. Des.*, vol. 130, no. 5, 2008, Art. no. 052304.

[16] P. Birkmeyer, A. G. Gillies, and R. S. Fearing, "CLASH: Climbing vertical loose cloth," in *Proc. IEEE/RSJ Int. Conf. Intell. Robots Syst.*, 2011, pp. 5087–5093.

[17] P. Holmes, R. J. Full, D. Koditschek, and J. Guckenheimer, "The dynamics of legged locomotion: Models, analyses, and challenges," *SIAM Rev.*, vol. 48, no. 2, pp. 207–304, 2006.